

# The Global Land Surface Satellite (GLASS) Product Suite

Shunlin Liang, Jie Cheng, Kun Jia, Bo Jiang, Qiang Liu, Zhiqiang Xiao, Yunjun Yao, Wenping Yuan, Xiaotong Zhang, Xiang Zhao, and Ji Zhou

**ABSTRACT:** The Global Land Surface Satellite (GLASS) product suite currently contains 12 products, including leaf area index, fraction of absorbed photosynthetically active radiation, fraction of green vegetation coverage, gross primary production, broadband albedo, broadband longwave emissivity, downward shortwave radiation and photosynthetically active radiation, land surface temperature, downward and upwelling thermal radiation, all-wave net radiation, and evapotranspiration. These products are generated from the Advanced Very High Resolution Radiometer and Moderate Resolution Imaging Spectroradiometer satellite data. Their unique features include long-term temporal coverage (many from 1981 to the present), high spatial resolutions of the surface radiation products (1 km and 0.05°), spatial continuities without missing pixels, and high quality and accuracy based on extensive validation using in situ measurements and intercomparisons with other existing satellite products. Moreover, the GLASS products are based on robust algorithms that have been published in peer-reviewed literature. Herein, we provide an overview of the algorithm development, product characteristics, and some preliminary applications of these products. We also describe the next steps, such as improving the existing GLASS products, generating more climate data records (CDRs), broadening product dissemination, and fostering their wider utilization. The GLASS products are freely available to the public.

**KEYWORDS:** Atmosphere-land interaction; Carbon cycle; Energy budget/balance; Radiative fluxes; Remote sensing; Satellite observations

<https://doi.org/10.1175/BAMS-D-18-0341.1>

Corresponding author: Shunlin Liang, [sliang@umd.edu](mailto:sliang@umd.edu)

In final form 9 September 2020

©2021 American Meteorological Society

For information regarding reuse of this content and general copyright information, consult the [AMS Copyright Policy](#).

**AFFILIATIONS:** Liang—Department of Geographical Sciences, University of Maryland, College Park, College Park, Maryland; Cheng,\* Jia,\* Jiang,\* Xiao,\* Yao,\* Zhang,\* and Zhao\*—State Key Laboratory of Remote Sensing Science, and Beijing Engineering Research Center for Global Land Remote Sensing Products, and Institute of Remote Sensing Science and Engineering, Faculty of Geographical Sciences, Beijing Normal University, Beijing, China; Liu\*—State Key Laboratory of Remote Sensing Science, and Beijing Engineering Research Center for Global Land Remote Sensing Products, and College of Global Change and Earth System Science, Beijing Normal University, Beijing, China; Yuan\*—School of Atmospheric Sciences, Sun Yat-sen University, Guangzhou, Guangdong, China; Zhou\*—School of Resources and Environment, Center for Information Geoscience, University of Electronic Science and Technology of China, Chengdu, China

\* Joint second coauthors, equally contributed to this paper.

The world is currently confronted with historically unprecedented environmental challenges, particularly those related to climate change. To better understand, monitor, and predict those changes, researchers need access to high-quality satellite products of different bio- and geophysical variables. Though several international space agencies produce high-level land products from different satellite observations, a major limitation of these products is their short temporal coverages, due to the fact that they are usually generated from observations made by a specific satellite sensor that has a limited life span. The remote sensing community has started to use the satellite data to generate climate data records (CDRs) of the essential climate variables (ECVs) defined by the Global Climate Observing System (GCOS; GCOS 2016), where CDRs are defined as time series of measurements with sufficient length, consistency, and continuity to determine climate variability and changes [National Research Council (NRC); NRC 2004]. However, not many land CDRs are currently available to the public, and more efforts to produce these land CDRs are critically needed.

Production of the Global Land Surface Satellite (GLASS) product suite began in 2009 with five initial products (Liang et al. 2013a,b), and continued development has led to more than a dozen products with improved accuracies and qualities over previous versions of the same products as well as other comparable products. Currently, 12 of these products are officially released. The GLASS products are primarily based on NASA's Advanced Very High Resolution Radiometer (AVHRR) long-term data record (LTDR) (<https://ltdr.modaps.eosdis.nasa.gov>) and Moderate Resolution Imaging Spectroradiometer (MODIS) data, in conjunction with other satellite data and ancillary information.

The characteristics of the 12 GLASS products (version 4), several of which correspond to ECVs, are outlined in Table 1. Compared to other existing satellite products, the GLASS products have several unique features: 1) the new products are not available from other sources (e.g., longwave broadband emissivity from both AVHRR and MODIS; downward longwave radiation from MODIS); 2) long-term time series data (many products span from 1981 to the present); 3) high spatial resolutions of the surface radiation products (1 km or 0.05°), which are much finer than other commonly used products ( $\geq 100$  km), such as the gridded Clouds and the Earth's Radiant Energy System (CERES) products (1°) and the Global Energy and Water Exchanges (GEWEX) surface radiation budget (SRB) products (280 km); 4) spatial continuities with no data gaps; and 5) higher accuracies and temporal consistencies based on direct validation using in situ measurements and product intercomparisons.

Algorithm development is critical for generating satellite products. The algorithms for the current version of the GLASS products are provided in each of the following sections, and additional details regarding comparisons with other algorithms can be found in a recent book (Liang and Wang 2019).

**Table 1. Characteristics of the GLASS products (version 4). Products 1, 2, 7, 8, 9 and 11 correspond to the essential climate variables (ECV). Both shortwave net radiation, which can be calculated by products 2 and 5, and longwave net radiation, which can be calculated by products 3, 7 and 8, are also ECVs.**

No.	Product	Temporal range	Temporal resolution	Spatial resolution
1	Leaf area index	1981–2018	8 days	0.05° from AVHRR, 500 m from MODIS
2	Broadband albedo	1981–2018	8 days	0.05° from AVHRR, 1 km from MODIS
3	Broadband emissivity	1981–2018	8 days	0.05° from AVHRR, 1 km from MODIS
4	Photosynthetically active radiation	2000–2018	Daily	0.05°
5	Downward shortwave radiation	2000–2018	Daytime/daily	0.05°
6	Downward longwave radiation	2000–2018	Instantaneous	1 km
7	All-wave net radiation	2000–2018	Daily	0.05°
8	Land surface temperature	1981–2000	Instantaneous	0.05°
9	Fraction absorbed photosynthetically active radiation	1981–2018	8 days	0.05° from AVHRR, 500 m from MODIS
10	Fractional vegetation cover	1981–2018	8 days	0.05° from AVHRR, 500 m from MODIS
11	Evapotranspiration	1981–2018	8 days	0.05° from AVHRR, 1 km from MODIS
12	Gross primary production	1981–2018	8 days	0.05° from AVHRR, 500 m from MODIS

The GLASS products have recently been used for different applications. To facilitate more extensive utilization of these products by the broader community, this paper provides an overview of the GLASS products’ characteristics, inversion algorithms, validation results and some preliminary applications. Ongoing activities focused on expanding and enhancing the GLASS products are also described.

### **Algorithm development, product characteristics, and applications**

**LAI.** Conceptually, there are both true leaf area index (LAI) and effective LAI. True LAI is defined as half of the total green leaf area per unit of horizontal ground surface area, while the effective LAI is the true LAI multiplied by the clumping index that quantifies the level of foliage grouping within distinct canopy structures relative to a random distribution (He et al. 2012). True LAI has been widely used by most models (Myneni et al. 2002).

The GLASS LAI product represents the true LAI that is generated using general regression neural networks (GRNNs) that are trained using the integrated satellite LAI time series and the MODIS surface reflectance data (Xiao et al. 2014) or the AVHRR surface reflectance data (Xiao et al. 2016c). The LAI time series integrates the MODIS (Myneni et al. 2002) and the Carbon Cycle and Change in Land Observational Products from an Ensemble of Satellites (CYCLOPES) (Baret et al. 2007) LAI products. Unlike existing neural network methods that use only satellite data acquired at a specific time to retrieve the LAI, the GLASS LAI algorithm uses preprocessed reflectance data from an entire year to train the GRNNs and to estimate the 1-yr LAI profile for each pixel since it is advantageous to use a surface reflectance time series rather than an individual reflectance value. Furthermore, the surface reflectance data from atmospheric correction are frequently contaminated by clouds, so preprocessing the surface reflectance data is an essential step in eliminating the impacts of this “noise.” Different algorithms have been developed to generate temporally continuous and smoothed surface reflectance time series (Tang et al. 2013; Xiao et al. 2015a, 2017b). Our experiences reveal that effective preprocessing techniques need to be employed to produce a high-quality LAI product.

Compared to other long-term LAI products, the GLASS LAI product has been shown to have higher quality and accuracy (Xiao et al. 2017a). Independent direct validation has also demonstrated that the GLASS LAI product exhibits the best accuracy, with  $R^2 = 0.70$  and root-mean-square error (RMSE) = 0.96 globally and  $R^2 = 0.94$  and RMSE = 0.61 over

China (X. L. Li et al. 2018). Another independent validation study also showed that the GLASS LAI product has the lowest uncertainty, followed by GEOV1 (the first version of Geoland2 satellite products) and MODIS for all the biome types tested (Xu et al. 2018). The high quality of the GLASS LAI product is characterized by its spatial and temporal continuity (no gaps or missing values), temporal stability, and representation of vegetation phenology.

Additionally the GLASS LAI products have been utilized to estimate other variables from satellite data, such as calculating the fraction of absorbed photosynthetically active radiation (FAPAR) (Xiao et al. 2016b, 2015b), fraction of vegetation coverage (Xiao et al. 2016a), broadband emissivity (BBE) over vegetated surfaces (Cheng et al. 2016; Meng et al. 2017), gross primary production (GPP) (Liu et al. 2018; Liu et al. 2015; Tian et al. 2017) and evapotranspiration (ET) (Sun et al. 2016; Tian et al. 2015), mapping wall-to-wall vegetation height in China (Huang et al. 2017), generating regional phenology (R. Wang et al. 2017), detecting forest disturbances (J. Wang et al. 2017), and characterizing the ecosystem dynamics within a watershed that has complex topography (Liu et al. 2017). A recently developed remote sensing data assimilation framework has also used the GLASS LAI product to simultaneously estimate a group of atmospheric and land surface parameters (Ma et al. 2017a,b, 2018; Shi et al. 2016, 2017; Xiao et al. 2015c).

The GLASS LAI products have also been used to drive various process-oriented models, such as the Lund–Potsdam–Jena dynamic global vegetation model (LPJ-DGVM), to achieve a better agreement between the estimated and observed GPP (Ma et al. 2017). A hydrological model used to determine the hydrological responses to reforestation has also utilized these LAI products (Liu et al. 2016).

The LAI products have also been used to evaluate land surface models (Bao et al. 2014; Druel et al. 2017; Guimberteau et al. 2018; Tesemma et al. 2015) and Earth system models (Huang et al. 2016), investigate vegetation–atmosphere interactions in order to evaluate the response of vegetation to the changing environment (Jiapaer et al. 2015), detect greening trends at different spatial scales (R. Q. Li et al. 2018; Piao et al. 2015; Z. Zhu et al. 2016), among others (Wang et al. 2018; Yu et al. 2018). The LAI products have also been assimilated into land surface models (Zhao et al. 2016).

**FAPAR.** FAPAR is a key biophysical variable that is directly related to the photosynthetic activity of plants, and is an indicator of the presence and productivity of living vegetation, as well as the intensity of the terrestrial carbon sink.

Instead of estimating the FAPAR directly from satellite data, the GLASS FAPAR products are derived from the GLASS LAI products and other auxiliary information (Xiao et al. 2015b). This method calculates the FAPAR values based mainly on the photosynthetically active radiation (PAR) transmittance of the entire canopy. An advantage of this approach is to ensure physical consistency between the LAI and FAPAR products. The GLASS FAPAR products represent the values at 1030 local time, which are close approximations of daily average FAPAR (Fensholt et al. 2004).

The long-term GLASS FAPAR product from the AVHRR was compared with two similar products: the National Centers for Environmental Information (NCEI) and the third-generation Global Inventory Monitoring and Modeling System (GIMMS3g) AVHRR FAPAR products. The GLASS product exhibits better quality and accuracy (Xiao et al. 2018).

The GLASS FAPAR products have been used in many studies. For example, H. Zhu et al. (2016) and L. Wang et al. (2017) demonstrated that substantial improvements in estimating the tower GPP were achieved by substituting the GLASS FAPAR product for the MODIS FAPAR product, especially for croplands. Hu et al. (2018) also incorporated the GLASS FAPAR product into their GPP calculations.

**FVC.** Fractional vegetation cover (FVC) generally refers to the fraction of green vegetation as seen from the nadir of the total statistical area. FVC is an important parameter for describing land surface vegetation conditions required by many land surface models, weather prediction models, regional and global climate models, hydrological models, and global change studies.

Multiple global FVC products have been generated from different satellite datasets; however, many require improvements in accuracy. For example, the GEOV1 FVC product is generally accurate (Camacho et al. 2013), but validation using data from an agricultural region indicates an overestimate of up to 0.2 (Mu et al. 2015).

The GLASS FVC product is based on machine learning methods that use training samples generated from globally distributed high-spatial-resolution satellite data (Jia et al. 2019). Initially, the GLASS FVC product algorithm for MODIS data were based on the GRNNs method (Jia et al. 2015). After comparing four machine learning methods, including back-propagation neural networks (BPNNs), GRNNs, support vector regression (SVR), and multivariate adaptive regression splines (MARS), the MARS method was chosen to produce the global FVC product from MODIS data. This was due to its high computational efficiency and reasonable accuracy (Yang et al. 2016).

The GLASS AVHRR FVC algorithm was based on the GLASS MODIS FVC product to achieve temporal consistency. First, 1-yr training samples were extracted globally where AVHRR reflectance data and the GLASS MODIS FVC product overlapped. The MARS model was then trained with the training samples and used to estimate the FVC from the preprocessed AVHRR reflectance data. Finally, the estimated FVC from the AVHRR data were linearly corrected based on the GLASS MODIS FVC to obtain the AVHRR FVC consistent with the GLASS MODIS FVC.

The GLASS FVC product has been evaluated by both direct validation and product inter-comparisons (Jia et al. 2019). Based on 44 reference datasets from the Validation of Land European Remote Sensing Instruments (VALERI) sites with various land-cover types, the RMSE of the GLASS FVC from the MODIS data is 0.157, which is comparable to that of the GEOV1 FVC product (RMSE = 0.166). The coefficient of determination ( $R^2$ ) of the GLASS MODIS FVC is 0.809, which is larger than that of the GEOV1 FVC product ( $R^2 = 0.775$ ). The GLASS AVHRR FVC product also has validation results ( $R^2 = 0.834$ , RMSE = 0.145) that are slightly superior to those of the GEOV1 FVC product from AVHRR data ( $R^2 = 0.799$ , RMSE = 0.174). A direct validation of the GLASS FVC product in an agricultural region based on a time series of field FVC measurements indicated that the performance of the GLASS FVC product ( $R^2 = 0.86$ , RMSE = 0.087) was better than the performance of the GEOV1 FVC product ( $R^2 = 0.71$ , RMSE = 0.193) using the same reference data (K. Jia et al. 2018). Other validation experiments have been conducted using estimates from high-resolution satellite data and ground measurements (K. Jia et al. 2018, 2016).

**DSR.** Surface downward shortwave radiation (DSR) is an essential component of the total energy exchanged between the atmosphere and the surface and is required by most land surface hydrological and ecological models. The earlier GLASS DSR product was based on an improved lookup table (LUT) method using multiple polar-orbiting and geostationary satellite datasets (Zhang et al. 2014). However, it was too time consuming to generate a long-term global DSR product using this method. To overcome this difficulty, the current GLASS DSR product is instead generated from the MODIS top-of-atmosphere (TOA) reflectance based on a direct-estimation method (Zhang et al. 2019).

The GLASS DSR product has a  $0.05^\circ$  spatial resolution and a daily temporal resolution. Validated by ground measurements collected at 525 stations from 2003 to 2015 around the

world, the GLASS monthly DSR has an overall bias of  $1.24 \text{ W m}^{-2}$  and an RMSE of  $21.16 \text{ W m}^{-2}$ . Moreover, the global land annual mean of the DSR was  $184.8 \text{ W m}^{-2}$ , with a standard deviation of  $0.8 \text{ W m}^{-2}$  over a 13-yr (2003–15) period.

**Downward PAR.** PAR is defined as the visible part (400–700 nm) of the DSR. It is an essential parameter in ecological modeling that controls the exchange of water vapor and carbon dioxide between vegetation and the atmosphere and is used to estimate global terrestrial vegetation productivity.

Currently, most global radiation products do not have a PAR component, so many users have to calculate PAR by multiplying the DSR by an empirical conversion constant of approximately 0.5 (Liang et al. 2006). The GLASS PAR product was previously produced using the LUT method (Liang et al. 2013b; Zhang et al. 2014). The current version of the PAR product is obtained from the GLASS DSR multiplied by a spatially and temporally variable conversion factor determined from the GEWEX-SRB V3.0 radiative flux products, in which DSR and PAR are provided separately. The accuracy of this method is comparable to that of the previous version of the product. Cai et al. (2014) demonstrated that the GLASS PAR product can produce better estimations of terrestrial GPP over China by comparing it with several other incident radiation products.

**Broadband albedo.** Land surface albedo describes the ratio of the upward to downward flux of solar radiation at the surface and is an important indicator of global environmental changes, such as urbanization, deforestation/afforestation, and Arctic sea ice retreat (Dickinson 1983).

Unlike the MODIS albedo products, which are based on inversions of the bidirectional reflectance distribution function (BRDF) model parameters, the GLASS albedo products are based on the direct-estimation method and represent surface albedo under general clear-sky atmospheric conditions. The GLASS albedo algorithm consists of two steps. The first step adopts the direct-estimation algorithm (Qu et al. 2014) to derive the intermediate albedo products, and the second step adopts the spatiotemporal filtering algorithm (N. Liu et al. 2013) to generate a smoothed and gap-free product.

The version 3 GLASS albedo product was released in 2012 (Q. Liu et al. 2013; Peng et al. 2015). The version 4 (V4) GLASS albedo products released in 2019 have been updated with regard to several aspects. In addition to the shortwave (SW) albedo, the products include visible (VIS) and near-infrared (NIR) albedo values. The snow/ice BRDF model has been updated (Qu et al. 2016), and a water surface BRDF model has been adopted for the ocean surface as well as for mixed pixels of water/sea ice (Feng et al. 2016). As a result, the quality and accuracy of the GLASS albedo products over ocean and sea ice areas have been improved (Qu et al. 2016; Feng et al. 2016).

The V4 GLASS shortwave albedo products were validated by tower-based observations from 53 spatially homogeneous global sites (Fig. 1). These measurements are part of the LaThuile Opened dataset from FLUXNET (Baldocchi et al. 2001). The RMSE was 0.052

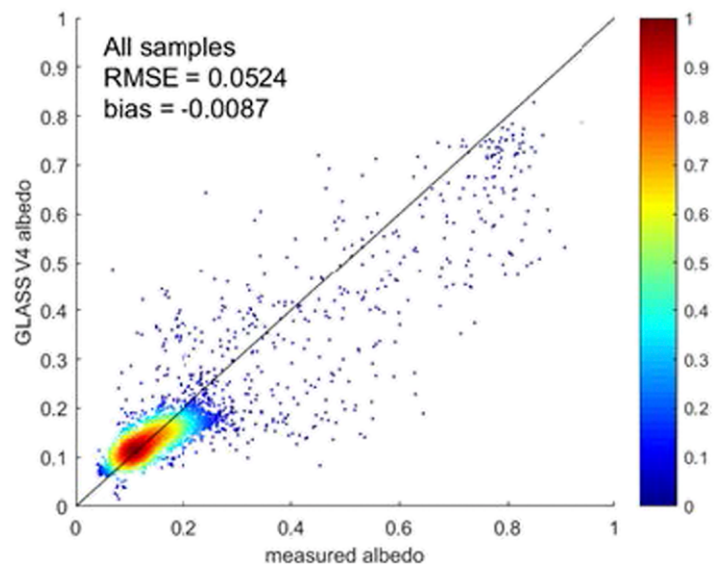


Fig. 1. Validation of the V4 GLASS shortwave albedo product (6,035 samples from the FLUXNET LaThuile Opened dataset).

for all matched samples. After screening out all the cloudy pixels, the RMSE was reduced to 0.037.

Since it is difficult to obtain ground measurements to directly validate visible and near-IR albedo, we compared these products with the MODIS (C6 MCD43A3) product. They are consistent over snow-free pixels, with RMSE values of 0.018 and 0.022, respectively. However, larger discrepancies were observed over snow/ice pixels, partially due to their differences in spatial resolution.

The GLASS albedo products have been used by many studies. For example, they have been used to calculate surface ET (Carter and Liang 2019), to determine radiative forcing due to land surface changes (Chen et al. 2016a,b, 2015; Hu et al. 2016, 2015; Li et al. 2015; Zhang and Liang 2014, 2018), and to evaluate environmental changes (Chen et al. 2017; He et al. 2014, 2013).

**LST.** Land surface temperature (LST) is a key parameter in many land processes. Thermal-infrared (TIR) remote sensing provides direct observation of thermal emission from the land surface, enabling the estimation of LST under clear-sky conditions. Numerous algorithms have been proposed, but a long-term global high-resolution LST satellite product has yet to be found, especially for data collected prior to the year 2000.

The GLASS LST product was recently released (Zhou et al. 2019; Ma et al. 2020) and differs from most of the current satellite LST products. The GLASS LST product is based on a multialgorithm ensemble approach, which combines nine split-window algorithms with the Bayesian model averaging (BMA) model. In the first phase, the GLASS LST product was produced for four discrete years with a spatial resolution of 0.05° for 1983 and 1993 and a spatial resolution of 1 km for 2003 and 2013. In the second phase, the product was expanded to cover 1981–2000 with a spatial resolution of 0.05°. In addition, the BMA model was replaced by a random forest based ensemble approach (Ma et al. 2020). The current GLASS LST product has also been corrected for the orbit drift effect.

The GLASS LST products have been validated by in situ LST measurements. In the preliminary validation stage (Zhou et al. 2019), the AVHRR LST product had an RMSE of 2.89 K when validated with measurements from the Barrow, Alaska (now known as Utqiagvik), site of the Baseline Surface Radiation Network (BSRN) (Driemel et al. 2018). For the MODIS LST product, validation with measurements from six grassland/cropland Surface Radiation Budget Network (SURFRAD) sites indicated that the mean RMSE values are 1.82–2.15 K at night for *Terra/Aqua* MODIS in 2003 and 2013. This accuracy is similar to that of the official MODIS LST product. In the validation stage, the AVHRR LST product was validated with historical in situ measurements from the SURFRAD data collected between 1995 and 2000, with a mean bias error (MBE) of 0.21 K and a range from –1.59 to 2.71 K (site dependent), and a standard deviation (STD) of 2.48 K with a range of 2.26–2.76 K (site dependent); and water data from the National Data Buoy Center (NDBC) collected between 1981 and 2000 that has an MBE of 0.11 K with a range from –0.01 to 0.26 K and a STD of 0.80 K with a range of 0.77–0.85 K.

A parallel effort has been undertaken to generate another GLASS AVHRR LST product from 1981 to 2000 using a generalized split-window algorithm (Liu et al. 2019). The major difference from the LST product described above is a further orbit drift correction that normalizes the estimated LST to the same local time based on the diurnal temperature cycle model and the Bayesian optimization algorithm. The validation results based on measurements from six SURFRAD sites produced RMSEs from 2.2 to 4.1 K and MBEs from –0.4 to 2.0 K.

**Broadband emissivity.** Surface thermal-infrared BBE is a key variable for calculating the

surface radiation budget, which is critical for addressing a variety of scientific and applied issues that are related to climate trends, weather prediction, hydrologic models, and biogeophysical models (Kustas et al. 2018; Liang et al. 2019; Wild et al. 2014). Jin and Liang (2006) demonstrated that incorporating a satellite-derived BBE product can significantly improve simulations with a coupled land surface and atmospheric model (National Center for Atmospheric Research Community Atmosphere Model + Community Land Model, version 2).

The GLASS BBE products represent the broadband emissivity between 8 and 13.5  $\mu\text{m}$ , which is the optimal spectral range for calculating longwave net radiation (Cheng et al. 2013). For the GLASS MODIS BBE product, land surfaces were classified into water, snow or ice, bare soil, vegetated surfaces, and transition zone, and their BBEs were calculated separately. The BBE of bare soil is estimated using the MODIS spectral reflective albedos (Cheng and Liang 2014), which are based on their linear relationship with the Advanced Spaceborne Thermal Emission and Reflection Radiometer (ASTER) spectral thermal emissivities that are converted to broadband emissivity. The vegetation BBE is calculated based on the leaf BBE, soil BBE, and LAI from a radiative transfer model (Cheng et al. 2016).

The GLASS AVHRR BBE product is generated from a similar algorithm, except that the AVHRR surface visible and near-infrared reflectances were used to replace the MODIS spectral albedos (Cheng and Liang 2013).

The GLASS BBE product was validated with field measurements of northern China from 2006 to 2011 (Dong et al. 2013). The differences over bare soils were within 0.02. The differences between the GLASS BBE derived from the MODIS data and measurements over fully vegetated surfaces were less than 0.005 (Cheng et al. 2016). Using ground measurements collected from six sites in the desert regions of North America in 2008, the mean BBE difference was 0.016 (Cheng and Liang 2014). Since no ground measurements were available to validate the GLASS AVHRR BBE before 2000, we checked the consistency between the 1-km MODIS BBE and the 0.05° AVHRR BBE products after 2000. The absolute value of mean difference and the RMSE were both less than 0.001. We also compared the GLASS BBE with the North American ASTER Land Surface Emissivity Database (Cheng et al. 2014) and found good agreement in both the summer and winter seasons.

The GLASS BBE products have been used to estimate evaporation (W. Yang et al. 2020) and ET (Ma et al. 2019), compare with the retrievals of a new inversion algorithm as a reference value (Ma et al. 2018), and to study climate impacts due to the widespread deployment of utility-scale solar energy installations (Li et al. 2017).

**Longwave downward and upward radiation.** The surface radiation budget is dominated by longwave radiation at night and in polar regions for most of the year. To estimate instantaneous clear-sky longwave upwelling (LWUP) and downward (LWDN) radiation from the MODIS data, we developed a hybrid model for LWUP (Cheng and Liang 2016) and for LWDN (Cheng et al. 2017a). For cloudy-sky conditions, we estimated the LWDN using the single layer cloud model (Forman and Margulis 2009) with inputs from the MODIS cloud product. The cloudy-sky LWUP was calculated from the GLASS BBE product and LST extracted from MODIS cloud product MOD06/MYD06.

For thermal radiation before 2000, we used the parameterization schemes to calculate clear-sky LWDN from reanalysis data (Cheng et al. 2019, 2020; Guo et al. 2019) and used the GLASS LST and BBE products to calculate LWUP.

Validation of the clear-sky GLASS MODIS products used three ground measurements from six networks at 141 globally distributed sites and showed that the bias and RMSE were  $-3.77$  and  $26.94 \text{ W m}^{-2}$ , respectively, for LWDN, and  $-4.33$  and  $18.15 \text{ W m}^{-2}$ , respectively, for LWUP. The bias and RMSE of the calculated longwave net radiation (LWNT) were  $0.70$  and  $26.7 \text{ W m}^{-2}$ , respectively, which are much better than those of other products (Zeng et al. 2020).



**All-wave net radiation.** The all-wave surface net radiation ( $R_n$ ) is the sum of the downward and upward fluxes of the shortwave ( $0.3\text{--}4\ \mu\text{m}$ ) and longwave ( $4\text{--}100\ \mu\text{m}$ ) spectra. The GLASS  $R_n$  product is produced based on its relationship with solar radiation and other meteorological information. After exploring linear regression models (Jiang et al. 2015) and multiple machine learning methods (Jiang et al. 2014), the MARS and random forest (RF) algorithms were selected to produce the GLASS daytime (Jiang et al. 2019) and daily  $R_n$  products. The DSR, normalized difference vegetation index (NDVI), and albedo from the GLASS products and meteorological values from the Modern-Era Retrospective Analysis for Research and Applications, version 2 (MERRA-2), reanalysis data (Gelaro et al. 2017) are the primary inputs.

The GLASS daytime and daily  $R_n$  products were validated with in situ measurements from more than 140 global sites. Comparisons were also made with CERES and two reanalysis products: the Japanese 55-year Reanalysis (JRA-55) and the European Centre for Medium-Range Weather Forecasts (ECMWF) interim reanalysis (ERA-Interim). The results in Table 2 show that the two satellite products (GLASS and CERES) are more accurate than the reanalysis datasets, and the GLASS  $R_n$  product exhibits the smallest RMSE and MBE on both daytime and daily scales.

**Table 2. Validation results of four daytime/daily  $R_n$  products against in situ measurements (36,733 samples).**

	Daily ( $n = 36,733$ )			Daytime ( $n = 52,176$ )		
	$R^2$	RMSE ( $\text{W m}^{-2}$ )	MBE ( $\text{W m}^{-2}$ )	$R^2$	RMSE ( $\text{W m}^{-2}$ )	MBE ( $\text{W m}^{-2}$ )
GLASS	0.82	28.99	-2.73	0.80	52.93	5.56
CERES_SYN1deg Ed3A	0.72	36.01	3.53	0.82	55.25	23.92
JRA-55	0.64	45.54	2.22	0.62	79.70	25.75
ERA-Interim	0.54	51.67	-5.96	0.64	74.18	20.86

We also calculated the average net radiation over land surfaces for the past decade. The GLASS net radiation product shows a similar temporal trend to the two reanalysis products, while the CERES product has a trend of opposite sign due to changes in the versions of input data (A. Jia et al. 2018).

**ET.** ET is a key variable linked to energy, water, and carbon exchange among the terrestrial biosphere, hydrosphere, and atmosphere. The GLASS ET product algorithm is based on the multimodel ensemble approach (Yao et al. 2014) and, in particular, the BMA method, which merges five process-based ET estimates, such as the MODIS ET product algorithm (MOD16) (Mu et al. 2011), the revised remote sensing-based Penman–Monteith ET algorithm (RRS-PM) (Yuan et al. 2010), the Priestley–Taylor-based ET algorithm (PT-JPL) (Fisher et al. 2008), modified satellite-based Priestley–Taylor ET algorithm (MS-PT) (Yao et al. 2013), and the semiempirical Penman ET algorithm of the University of Maryland (UMD-SEMI) (Wang et al. 2010).

The validation of the GLASS ET product used ground measurements from 240 eddy covariance flux tower sites and illustrated that the GLASS ET product using the BMA method enhances the latent heat flux (LE) estimates, with a smaller RMSE ( $35.3\ \text{W m}^{-2}$ ) and a larger average  $R^2$  (0.75) than the MODIS ET product (RMSE =  $45.3\ \text{W m}^{-2}$ ,  $R^2 = 0.62$ ) using the individual algorithms driven by the tower-specific and MERRA-2 meteorological data. Additionally, L. Song et al. (2018) compared five major satellite ET products over the Heihe River basin in China and found that the GLASS ET product was more accurate than the individual model calculations.

**GPP.** Vegetation GPP refers to the rate at which green plants in the ecosystem produce organic matter by assimilating carbon dioxide using solar energy through photosynthesis. The GLASS GPP algorithm originates from the Eddy Covariance–Light Use Efficiency (EC-LUE) model (Yuan et al. 2007). The original EC-LUE model is driven by only four variables: NDVI, PAR, air temperature, and the Bowen ratio of sensible to latent heat flux. The later version of the EC-LUE model substitutes the ratio of ET to net radiation for the Bowen ratio, and revises the remote sensing Penman–Monteith (RS-PM) model to quantify ET (Yuan et al. 2010). To accurately indicate the long-term changes in GPP, the GLASS GPP product uses the latest version of the EC-LUE model that integrates the impacts of several environmental variables: atmospheric CO<sub>2</sub> concentrations, direct and diffuse radiation fluxes, and atmospheric water vapor pressure deficit (VPD) (Yuan et al. 2019).

The EC-LUE model has been validated throughout North America, Europe and East Asia using measurements from eddy covariance towers (Li et al. 2013; Yuan et al. 2014, 2010, 2007). The validations show that the EC-LUE model can successfully reproduce the spatial and temporal variabilities of GPP over various ecosystem types.

Several model comparisons also indicate the superior performance of the EC-LUE model over other LUE models. Previous studies compared the EC-LUE model and the MODIS GPP products based on measurements from eddy covariance towers in southeastern China and found that the EC-LUE model performed better than the MODIS algorithms (Xu et al. 2013). A recent study compared eight satellite-based GPP models over various major grassland ecosystem types and found that the EC-LUE model had the best performance (W. Jia et al. 2018). Evaluation at 85 eddy covariance towers, distributed globally, demonstrated that the GLASS GPP product is able to represent interannual variations and long-term trends because it integrates important environmental variables (Zheng et al. 2020).

The GLASS GPP product has been widely used to examine the spatial and temporal variations in GPP (Han et al. 2015; Hu et al. 2018; Ma et al. 2015; Wang et al. 2015; Xu et al. 2013). For example, Yuan et al. (2019) used the GLASS GPP product to investigate the impacts of atmospheric VPD on global terrestrial GPP and found persistent widespread decreases in GPP after the late 1990s due to increases in VPD, which offset the positive CO<sub>2</sub> fertilization effect. In addition, the GLASS GPP algorithm has been used to develop and improve other GPP models (Kanniah et al. 2009; Pasquato et al. 2015; Restrepo-Coupe et al. 2013; Verma et al. 2015).

### **Production and distributions**

The GLASS product production system, which includes high-performance computing capabilities, is located at Beijing Normal University (Zhao et al. 2013). The system includes processing, management and data service modules and currently stores more than 3 PB of data.

The HDF-EOS file format is used to store the GLASS products. In addition, we use the JPG format to display product thumbnails and the XML format to store product metadata. All of the products are provided in the sinusoidal map projection for the MODIS data at 500-m or 1-km spatial resolution, and in the geographic latitude/longitude map projection for the AVHRR data at a 0.05° spatial resolution. All products are also aggregated and distributed at 0.05° or coarser resolution.

The GLASS products can be downloaded from the following websites: [www.glass.umd.edu](http://www.glass.umd.edu) and [www.geodata.cn/thematicView/GLASS.html](http://www.geodata.cn/thematicView/GLASS.html). The first website is in English, and the second one is mainly in Chinese.

### **Next steps**

We continue to improve the GLASS products in the following ways:

- 1) Enhancing the spatial resolutions of the current products. Several products (e.g., shortwave albedo, LAI, and FVC) will ultimately have a spatial resolution of 250 m since 2000. A parallel project is being undertaken to generate some of these products, as well as new products, at a 30-m resolution, which are denoted as high-resolution GLASS (Hi-GLASS) products.
- 2) Improving the accuracy and quality of the current products by using advanced machine learning algorithms and more satellite data sources (e.g., European and Chinese satellite data).
- 3) Expanding the number of products. Efforts are being made to generate more land, atmospheric and oceanic climate data records (CDRs) from different satellite observations. Many algorithms for generating these products have been developed, including those for top-of-atmosphere (TOA) shortwave albedo (Z. Song et al. 2018; Wang and Liang 2016, 2017), ocean shortwave albedo (Feng et al. 2016; Qu et al. 2016) and longwave emissivity (Cheng et al. 2017b), land surface NDVI (Xiao et al. 2015a, 2017b), fractional snow cover (Chen et al. 2018), surface air temperature (Rao et al. 2019), and forest above-ground biomass (L. Yang et al. 2020). Some of these products correspond to ECVs and are available upon request.
- 4) Broadening dissemination of the GLASS products. In addition to giving more presentations at conferences, workshops and summer schools, we are improving the web user interface for effective and efficient data downloading and are distributing GLASS product information to global users through the Global Earth Observation System of Systems (GEOSS) data portal (<https://www.geoportal.org/>).
- 5) Fostering greater utilization of the GLASS products. We are developing collaborations between the GLASS product team and other research projects and have planned the first GLASS user conference for the summer of 2021.

**Acknowledgments.** This work was partially supported by the Chinese Grand Research Program on Climate Change and Response through Grant 2016YFA0600103 and the National Earth System Science Data Center, National Science & Technology Infrastructure of China (<http://www.geodata.cn>). Many colleagues and graduate students have contributed to the development of the GLASS products. We thank the anonymous reviewers for their valuable comments and suggestions that have greatly improved the presentation of this paper.

## References

- Baldocchi, D., and Coauthors, 2001: FLUXNET: A new tool to study the temporal and spatial variability of ecosystem-scale carbon dioxide, water vapor, and energy flux densities. *Bull. Amer. Meteor. Soc.*, **82**, 2415–2434, [https://doi.org/10.1175/1520-0477\(2001\)082<2415:FANTTS>2.3.CO;2](https://doi.org/10.1175/1520-0477(2001)082<2415:FANTTS>2.3.CO;2).
- Bao, Y., and Coauthors, 2014: Evaluation of CMIP5 Earth system models in reproducing leaf area index and vegetation cover over the Tibetan Plateau. *J. Meteor. Res.*, **28**, 1041–1060, <https://doi.org/10.1007/s13351-014-4023-5>.
- Baret, F., and Coauthors, 2007: LAI, FAPAR and fCOVER CYCLOPES global products derived from VEGETATION. Part I: Principles of the algorithm. *Remote Sens. Environ.*, **110**, 275–286, <https://doi.org/10.1016/j.rse.2007.02.018>.
- Cai, W., and Coauthors, 2014: Improved estimations of gross primary production using satellite-derived photosynthetically active radiation. *J. Geophys. Res. Biogeosci.*, **119**, 2013JG002456, <https://doi.org/10.1002/2013JG002456>.
- Camacho, F., J. Cemicharo, R. Lacaze, F. Baret, and M. Weiss, 2013: GEOV1: LAI, FAPAR essential climate variables and fCOVER global time series capitalizing over existing products. Part II: Validation and intercomparison with reference products. *Remote Sens. Environ.*, **137**, 310–329, <https://doi.org/10.1016/j.rse.2013.02.030>.
- Carter, C., and S. Liang, 2019: Evaluation of ten machine learning methods for estimating terrestrial evapotranspiration from remote sensing. *Int. J. Appl. Earth Obs. Geoinf.*, **78**, 86–92, <https://doi.org/10.1016/j.jag.2019.01.020>.
- Chen, X., S. Liang, Y. Cao, T. He, and D. Wang, 2015: Observed contrast changes in snow cover phenology in northern middle and high latitudes from 2001–2014. *Sci. Rep.*, **5**, 16820, <https://doi.org/10.1038/srep16820>.
- , ———, and ———, 2016a: Satellite observed changes in the Northern Hemisphere snow cover phenology and the associated radiative forcing and feedback between 1982 and 2013. *Environ. Res. Lett.*, **11**, 084002, <https://doi.org/10.1088/1748-9326/11/8/084002>.
- , ———, ———, and T. He, 2016b: Distribution, attribution, and radiative forcing of snow cover changes over China from 1982 to 2013. *Climatic Change*, **137**, 363–377, <https://doi.org/10.1007/s10584-016-1688-z>.
- , ———, and ———, 2017: Sensitivity of summer drying to spring snow-albedo feedback throughout the Northern Hemisphere from satellite observations. *IEEE Geosci. Remote Sens. Lett.*, **14**, 2345–2349, <https://doi.org/10.1109/LGRS.2017.2764543>.
- , D. Long, S. Liang, L. He, C. Zeng, X. Hao, and Y. Hong, 2018: Developing a composite daily snow cover extent record over the Tibetan Plateau from 1981 to 2016 using multisource data. *Remote Sens. Environ.*, **215**, 284–299, <https://doi.org/10.1016/j.rse.2018.06.021>.
- Cheng, J., and S. Liang, 2013: Estimating global land surface broadband thermal-infrared emissivity using Advanced Very High Resolution Radiometer optical data. *Int. J. Digital Earth*, **6**, 34–49, <https://doi.org/10.1080/17538947.2013.783129>.
- , and ———, 2014: Estimating the broadband longwave emissivity of global bare soil from the MODIS shortwave albedo product. *J. Geophys. Res. Atmos.*, **119**, 614–634, <https://doi.org/10.1002/2013JD020689>.
- , and ———, 2016: Global estimates for high-spatial-resolution clear-sky land surface upwelling longwave radiation from MODIS data. *IEEE Trans. Geosci. Remote Sens.*, **54**, 4115–4129, <https://doi.org/10.1109/TGRS.2016.2537650>.
- , ———, Y. Yao, and X. Zhang, 2013: Estimating the optimal broadband emissivity spectral range for calculating surface longwave net radiation. *IEEE Geosci. Remote Sens. Lett.*, **10**, 401–405, <https://doi.org/10.1109/LGRS.2012.2206367>.
- , ———, ———, B. Ren, L. Shi, and H. Liu, 2014: A comparative study of three land surface broadband emissivity datasets from satellite data. *Remote Sens.*, **6**, 111–134, <https://doi.org/10.3390/rs6010111>.
- , ———, W. Verhoef, L. Shi, and Q. Liu, 2016: Estimating the hemispherical broadband longwave emissivity of global vegetated surfaces using a radiative transfer model. *IEEE Trans. Geosci. Remote Sens.*, **54**, 905–917, <https://doi.org/10.1109/TGRS.2015.2469535>.
- , ———, and W. Wang, 2017a: Surface downward longwave radiation. *Earth's Energy Budget*, S. Liang, Ed., Vol. 5, *Comprehensive Remote Sensing*, Elsevier, 196–216.
- , X. Cheng, S. Liang, R. Niclòs, A. Nie, and Q. Liu, 2017b: A lookup table-based method for estimating sea surface hemispherical broadband emissivity values (8–13.5 mm). *Remote Sens.*, **9**, 245, <https://doi.org/10.3390/RS9030245>.
- , F. Yang, and Y. Guo, 2019: A comparative study of bulk parameterization schemes for estimating cloudy-sky surface downward longwave radiation. *Remote Sens.*, **11**, 528, <https://doi.org/10.3390/rs11050528>.
- , S. Liang, and J. Shi, 2020: Impact of air temperature inversion on the clear-sky surface downward longwave radiation estimation. *IEEE Trans. Geosci. Remote Sens.*, **58**, 4796–4802, <https://doi.org/10.1109/TGRS.2020.2967432>.
- Dickinson, R. E., 1983: Land surface processes and climate-surface albedos and energy balance. *Advances in Geophysics*, Vol. 25, Academic Press, 305–353, [https://doi.org/10.1016/S0065-2687\(08\)60176-4](https://doi.org/10.1016/S0065-2687(08)60176-4).
- Dong, L., J. Hu, S. Tang, and M. Min, 2013: Field validation of GLASS land surface broadband emissivity database using pseudo-invariant sand dune sites in north of China. *Int. J. Digital Earth*, **6**, 96–112, <https://doi.org/10.1080/17538947.2013.822573>.
- Driemel, A., and Coauthors, 2018: Baseline Surface Radiation Network (BSRN): Structure and data description (1992–2017). *Earth Syst. Sci. Data*, **10**, 1491–1501, <https://doi.org/10.5194/essd-10-1491-2018>.
- Druel, A., and Coauthors, 2017: Towards a more detailed representation of high-latitude vegetation in the global land surface model ORCHIDEE (ORC-HL-VEGv1.0). *Geosci. Model Dev.*, **10**, 4693–4722, <https://doi.org/10.5194/gmd-10-4693-2017>.
- Feng, Y., Q. Liu, Y. Qu, and S. Liang, 2016: Estimation of the ocean water albedo from remote sensing and meteorological reanalysis data. *IEEE Trans. Geosci. Remote Sens.*, **54**, 850–868, <https://doi.org/10.1109/TGRS.2015.2468054>.
- Fensholt, R., I. Sandholt, and M. S. Rasmussen, 2004: Evaluation of MODIS LAI, fAPAR and the relation between fAPAR and NDVI in a semi-arid environment using in situ measurements. *Remote Sens. Environ.*, **91**, 490–507, <https://doi.org/10.1016/j.rse.2004.04.009>.
- Fisher, J. B., K. P. Tu, and D. D. Baldocchi, 2008: Global estimates of the land-atmosphere water flux based on monthly AVHRR and ISLSCP-II data, validated at 16 FLUXNET sites. *Remote Sens. Environ.*, **112**, 901–919, <https://doi.org/10.1016/j.rse.2007.06.025>.
- Forman, B., and S. Margulis, 2009: High-resolution satellite-based cloud-coupled estimates of total downwelling surface radiation for hydrologic modelling applications. *Hydrol. Earth Syst. Sci.*, **13**, 969–986, <https://doi.org/10.5194/hess-13-969-2009>.
- GCOS, 2016: The Global Observing System for Climate: Implementation needs. GCOS Rep. GCOS-200, 342 pp.
- Gelaro, R., and Coauthors, 2017: The Modern-Era Retrospective Analysis for Research and Applications, version 2 (MERRA-2). *J. Climate*, **30**, 5419–5454, <https://doi.org/10.1175/JCLI-D-16-0758.1>.
- Guimberteau, M., and Coauthors, 2018: ORCHIDEE-MICT (v8.4.1), a land surface model for the high latitudes: Model description and validation. *Geosci. Model Dev.*, **11**, 121–163, <https://doi.org/10.5194/gmd-11-121-2018>.
- Guo, Y., J. Cheng, and S. Liang, 2019: Comprehensive assessment of parameterization methods for estimating clear-sky surface downward longwave radiation. *Theor. Appl. Climatol.*, **135**, 1045–1058, <https://doi.org/10.1007/S00704-018-2423-7>.
- Han, F., and Coauthors, 2015: Effects of climate change on phenology and primary productivity in the desert steppe of Inner Mongolia. *J. Arid Land*, **7**, 251–263, <https://doi.org/10.1007/s40333-014-0042-4>.
- He, L., J. M. Chen, J. Pisek, C. B. Schaaf, and A. H. Strahler, 2012: Global clumping index map derived from the MODIS BRDF product. *Remote Sens. Environ.*, **119**, 118–130, <https://doi.org/10.1016/j.rse.2011.12.008>.
- He, T., S. Liang, Y. Yu, Q. Liu, and F. Gao, 2013: Greenland surface albedo changes 1981–2012 from satellite observations. *Environ. Res. Lett.*, **8**, 044043, <https://doi.org/10.1088/1748-9326/8/4/044043>.
- , ———, and D.-X. Song, 2014: Analysis of global land surface albedo climatology and spatial-temporal variation during 1981–2010 from multiple

- satellite products. *J. Geophys. Res. Atmos.*, **119**, 10 281–10 298, <https://doi.org/10.1002/2014JD021667>.
- Hu, L., W. Fan, H. Ren, S. Liu, Y. Cui, and P. Zhao, 2018: Spatiotemporal dynamics in vegetation GPP over the Great Khingan mountains using GLASS products from 1982 to 2015. *Remote Sens.*, **10**, 488, <https://doi.org/10.3390/rs10030488>.
- Hu, Y., M. Hou, G. Jia, X. Zhang, R. Xu, and Y. He, 2015: Comparison of three different methods to identify fractional urban signals for improving climate modelling. *Int. J. Remote Sens.*, **36**, 3274–3292, <https://doi.org/10.1080/01431161.2015.1042593>.
- , G. Jia, C. Pohl, X. Zhang, and J. van Genderen, 2016: Assessing surface albedo change and its induced radiation budget under rapid urbanization with Landsat and GLASS data. *Theor. Appl. Climatol.*, **123**, 711–722, <https://doi.org/10.1007/s00704-015-1385-2>.
- Huang, H., C. Liu, X. Wang, G. S. Biging, Y. Chen, J. Yang, and P. Gong, 2017: Mapping vegetation heights in China using slope correction ICESat data, SRTM, MODIS-derived and climate data. *ISPRS J. Photogramm. Remote Sens.*, **129**, 189–199, <https://doi.org/10.1016/j.isprsjprs.2017.04.020>.
- Huang, Y., S. Gerber, T. Huang, and J. W. Lichstein, 2016: Evaluating the drought response of CMIP5 models using global gross primary productivity, leaf area, precipitation, and soil moisture data. *Global Biogeochem. Cycles*, **30**, 1827–1846, <https://doi.org/10.1002/2016GB005480>.
- Jia, A., S. Liang, B. Jiang, X. Zhang, and G. Wang, 2018: Comprehensive assessment of global surface net radiation products and uncertainty analysis. *J. Geophys. Res. Atmos.*, **123**, 1970–1989, <https://doi.org/10.1002/2017JD027903>.
- Jia, K., and Coauthors, 2015: Global land surface fractional vegetation cover estimation using general regression neural networks from MODIS surface reflectance. *IEEE Trans. Geosci. Remote Sens.*, **53**, 4787–4796, <https://doi.org/10.1109/TGRS.2015.2409563>.
- , and Coauthors, 2016: Fractional vegetation cover estimation algorithm for Chinese GF-1 wide field view data. *Remote Sens. Environ.*, **177**, 184–191, <https://doi.org/10.1016/j.rse.2016.02.019>.
- , S. L. Liang, X. Q. Wei, Y. J. Yao, L. Q. Yang, X. T. Zhang, and D. Y. Liu, 2018: Validation of Global Land Surface Satellite (GLASS) fractional vegetation cover product from MODIS data in an agricultural region. *Remote Sens. Lett.*, **9**, 847–856, <https://doi.org/10.1080/2150704X.2018.1484958>.
- , and Coauthors, 2019: Long-term Global Land Surface Satellite (GLASS) fractional vegetation cover product derived from MODIS and AVHRR data. *IEEE J. Sel. Top. Appl. Earth Obs. Remote Sens.*, **12**, 508–518, <https://doi.org/10.1109/JSTARS.2018.2854293>.
- Jia, W., M. Liu, D. Wang, H. He, P. Shi, Y. Li, and Y. Wang, 2018: Uncertainty in simulating regional gross primary productivity from satellite-based models over northern China grassland. *Ecol. Indic.*, **88**, 134–143, <https://doi.org/10.1016/j.ecolind.2018.01.028>.
- Jiang, B., Y. Zhang, S. Liang, X. Zhang, and Z. Xiao, 2014: Surface daytime net radiation estimation using artificial neural networks. *Remote Sens.*, **6**, 11 031–11 050, <https://doi.org/10.3390/rs6111031>.
- , and Coauthors, 2015: Empirical estimation of daytime net radiation from shortwave radiation and ancillary information. *Agric. For. Meteorol.*, **211**–212, 23–36, <https://doi.org/10.1016/j.agrformet.2015.05.003>.
- , and Coauthors, 2019: Validation of the surface daytime net radiation product from version 4.0 GLASS product suite. *IEEE Geosci. Remote Sens. Lett.*, **16**, 509–513, <https://doi.org/10.1109/LGRS.2018.2877625>.
- Jiapaer, G., S. Liang, Q. X. Yi, and J. P. Liu, 2015: Vegetation dynamics and responses to recent climate change in Xinjiang using leaf area index as an indicator. *Ecol. Indic.*, **58**, 64–76, <https://doi.org/10.1016/j.ecolind.2015.05.036>.
- Jin, M., and S. Liang, 2006: Improve land surface emissivity parameter for land surface models using global remote sensing observations. *J. Climate*, **19**, 2867–2881, <https://doi.org/10.1175/JCLI3720.1>.
- Kanniah, K. D., J. Beringer, L. B. Hutley, N. J. Tapper, and X. Zhu, 2009: Evaluation of collections 4 and 5 of the MODIS gross primary productivity product and algorithm improvement at a tropical savanna site in northern Australia. *Remote Sens. Environ.*, **113**, 1808–1822, <https://doi.org/10.1016/j.rse.2009.04.013>.
- Kustas, W. P., and Coauthors, 2018: The Grape Remote Sensing Atmospheric Profile and Evapotranspiration Experiment. *Bull. Amer. Meteor. Soc.*, **99**, 1791–1812, <https://doi.org/10.1175/BAMS-D-16-0244.1>.
- Li, R. Q., Y. H. Gao, D. L. Chen, Y. X. Zhang, and S. S. Li, 2018: Contrasting vegetation changes in dry and humid regions of the Tibetan Plateau over recent decades. *Sci. Cold Arid Reg.*, **10**, 482–492, [www.scar.ac.cn/EN/Y2018/V10/I6/482](http://www.scar.ac.cn/EN/Y2018/V10/I6/482).
- Li, S., J. Weigand, and S. Ganguly, 2017: The potential for climate impacts from widespread deployment of utility-scale solar energy installations: An environmental remote sensing perspective. *J. Remote Sensing GIS*, **6**, 51963947, <https://doi.org/10.4172/2469-4134.1000190>.
- Li, X., and Coauthors, 2013: Estimation of gross primary production over the terrestrial ecosystems in China. *Ecol. Modell.*, **261**–262, 80–92, <https://doi.org/10.1016/j.ecolmodel.2013.03.024>.
- Li, X. L., H. Lu, L. Yu, and K. Yang, 2018: Comparison of the spatial characteristics of four remotely sensed leaf area index products over China: Direct validation and relative uncertainties. *Remote Sens.*, **10**, 26, <https://doi.org/10.3390/RS10010148>.
- Li, Y., M. Zhao, S. Motesharrei, Q. Mu, E. Kalnay, and S. Li, 2015: Local cooling and warming effects of forests based on satellite observations. *Nat. Commun.*, **6**, 6603, <https://doi.org/10.1038/ncomms7603>.
- Liang, S., and J. Wang, 2019: *Advanced Remote Sensing: Terrestrial Information Extraction and Applications*. 2nd ed. Elsevier, 985 pp.
- , T. Zheng, R. Liu, H. Fang, S. C. Tsay, and S. Running, 2006: Mapping incident photosynthetically active radiation (PAR) from MODIS data. *J. Geophys. Res. Atmos.*, **111**, D15208, <https://doi.org/10.11029/12005JD006730>.
- , X. Zhang, Z. Xiao, J. Cheng, Q. Liu, and X. Zhao, 2013a: *Global Land Surface Satellite (GLASS) Products: Algorithms, Validation and Analysis*. Springer, 171 pp.
- , and Coauthors, 2013b: A long-term Global Land Surface Satellite (GLASS) dataset for environmental studies. *Int. J. Digital Earth*, **6**, 5–33, <https://doi.org/10.1080/17538947.2013.805262>.
- , D. Wang, T. He, and Y. Yu, 2019: Remote sensing of Earth's energy budget: Synthesis and review. *Int. J. Digital Earth*, **12**, 737–780, <https://doi.org/10.1080/17538947.2019.1597189>.
- Liu, N., Q. Liu, L. Wang, S. Liang, J. Wen, Y. Qu, and S. Liu, 2013: A statistics-based temporal filter algorithm to map spatiotemporally continuous shortwave albedo from MODIS data. *Hydrol. Earth Syst. Sci.*, **17**, 2121–2129, <https://doi.org/10.5194/hess-17-2121-2013>.
- Liu, P., L. Hao, C. Pan, D. Zhou, Y. Liu, and G. Sun, 2017: Combined effects of climate and land management on watershed vegetation dynamics in an arid environment. *Sci. Total Environ.*, **589**, 73–88, <https://doi.org/10.1016/j.scitotenv.2017.02.210>.
- Liu, Q., L. Wang, Y. Qu, N. Liu, S. Liu, H. Tang, and S. Liang, 2013: Preliminary evaluation of the long-term GLASS albedo product. *Int. J. Digital Earth*, **6**, 69–95, <https://doi.org/10.1080/17538947.2013.804601>.
- Liu, W., and Coauthors, 2016: Hydrological recovery in two large forested watersheds of southeastern China: The importance of watershed properties in determining hydrological responses to reforestation. *Hydrol. Earth Syst. Sci.*, **20**, 4747–4756, <https://doi.org/10.5194/hess-20-4747-2016>.
- Liu, X., B.-H. Tang, G. Yan, Z.-L. Li, and S. Liang, 2019: Retrieval of global orbit drift corrected land surface temperature from long-term AVHRR data. *Remote Sens.*, **11**, 2843, <https://doi.org/10.3390/rs11232843>.
- Liu, Y. B., and Coauthors, 2018: Satellite-derived LAI products exhibit large discrepancies and can lead to substantial uncertainty in simulated carbon and water fluxes. *Remote Sens. Environ.*, **206**, 174–188, <https://doi.org/10.1016/j.rse.2017.12.024>.
- Liu, Z., Q. Shao, and J. Liu, 2015: The performances of MODIS-GPP and-ET products in China and their sensitivity to input data (FPAR/LAI). *Remote Sens.*, **7**, 135–152, <https://doi.org/10.3390/rs70100135>.
- Ma, H., Q. Liu, S. Liang, and Z. Xiao, 2017a: Simultaneous estimation of leaf area index, fraction of absorbed photosynthetically active radiation and surface albedo from multiple-satellite data. *IEEE Trans. Geosci. Remote Sens.*, **55**, 4334–4354, <https://doi.org/10.1109/TGRS.2017.2691542>.

- , S. Liang, Z. Xiao, and H. Shi, 2017b: Simultaneous inversion of multiple land surface parameters from MODIS optical-thermal observations. *ISPRS J. Photogramm. Remote Sens.*, **128**, 240–254, <https://doi.org/10.1016/j.isprsjprs.2017.04.007>.
- , ——, ——, and D. Wang, 2018: Simultaneous estimation of multiple land surface parameters from VIIRS optical-thermal data. *IEEE Geosci. Remote Sens. Lett.*, **15**, 156–160, <https://doi.org/10.1109/LGRS.2017.2779040>.
- Ma, J., X. Yan, W. Dong, and J. Chou, 2015: Gross primary production of global forest ecosystems has been overestimated. *Sci. Rep.*, **5**, 10820, <https://doi.org/10.1038/srep10820>.
- , J. Zhou, F.-M. Göttsche, S. Liang, S. Wang, and M. Li, 2020: A global long-term (1981–2000) land surface temperature product for NOAA AVHRR. *Earth Syst. Sci. Data*, **12**, 3247–3268, <https://doi.org/10.5194/essd-12-3247-2020>.
- Ma, N., J. Szilagyi, Y. Zhang, and W. Liu, 2019: Complementary-relationship-based modeling of terrestrial evapotranspiration across China during 1982–2012: Validations and spatiotemporal analyses. *J. Geophys. Res. Atmos.*, **124**, 4326–4351, <https://doi.org/10.1029/2018JD029850>.
- Ma, R., and Coauthors, 2017: Assimilation of remotely-sensed leaf area index into a dynamic vegetation model for gross primary productivity estimation. *Remote Sens.*, **9**, 188, <https://doi.org/10.3390/rs9030188>.
- Meng, X., J. Cheng, and S. Liang, 2017: Estimating land surface temperature from Feng Yun-3C/MERSI data using a new land surface emissivity scheme. *Remote Sens.*, **9**, 1247, <https://doi.org/10.3390/rs9121247>.
- Mu, Q., M. Zhao, and S. W. Running, 2011: Improvements to a MODIS global terrestrial evapotranspiration algorithm. *Remote Sens. Environ.*, **115**, 1781–1800, <https://doi.org/10.1016/j.rse.2011.02.019>.
- Mu, X., S. Huang, H. Ren, G. Yan, W. Song, and G. Ruan, 2015: Validating GEOV1 fractional vegetation cover derived from coarse-resolution remote sensing images over croplands. *IEEE J. Sel. Top. Appl. Earth Obs. Remote Sens.*, **8**, 439–446, <https://doi.org/10.1109/JSTARS.2014.2342257>.
- Myneni, R. B., and Coauthors, 2002: Global products of vegetation leaf area and fraction absorbed PAR from year one of MODIS data. *Remote Sens. Environ.*, **83**, 214–231, [https://doi.org/10.1016/S0034-4257\(02\)00074-3](https://doi.org/10.1016/S0034-4257(02)00074-3).
- NRC, 2004: *Climate Data Records from Environmental Satellites: Interim Report*. National Academies Press, 150 pp.
- Pasquato, M., C. Medici, A. D. Friend, and F. Francés, 2015: Comparing two approaches for parsimonious vegetation modelling in semiarid regions using satellite data. *Ecohydrology*, **8**, 1024–1036, <https://doi.org/10.1002/eco.1559>.
- Peng, J., and Coauthors, 2015: Multi-scale validation strategy for satellite albedo products and its uncertainty analysis. *Sci. China Earth Sci.*, **58**, 573–588, <https://doi.org/10.1007/s11430-014-4997-y>.
- Piao, S. L., and Coauthors, 2015: Detection and attribution of vegetation greening trend in China over the last 30 years. *Global Change Biol.*, **21**, 1601–1609, <https://doi.org/10.1111/gcb.12795>.
- Qu, Y., Q. Liu, S. Liang, L. Wang, N. Liu, and S. Liu, 2014: Improved direct-estimation algorithm for mapping daily land-surface broadband albedo from MODIS data. *IEEE Trans. Geosci. Remote Sens.*, **52**, 907–919, <https://doi.org/10.1109/TGRS.2013.2245670>.
- , S. Liang, Q. Liu, X. Li, Y. Feng, and S. Liu, 2016: Estimating Arctic sea-ice shortwave albedo from MODIS data. *Remote Sens. Environ.*, **186**, 32–46, <https://doi.org/10.1016/j.rse.2016.08.015>.
- Rao, Y., and Coauthors, 2019: Estimating daily average surface air temperature using satellite land surface temperature and top-of-atmosphere radiation products over the Tibetan Plateau. *Remote Sens. Environ.*, **234**, 111462, <https://doi.org/10.1016/j.rse.2019.111462>.
- Restrepo-Coupe, N., and Coauthors, 2013: What drives the seasonality of photosynthesis across the Amazon basin? A cross-site analysis of eddy flux tower measurements from the Brasil flux network. *Agric. For. Meteorol.*, **182–183**, 128–144, <https://doi.org/10.1016/j.agrformet.2013.04.031>.
- Shi, H., Z. Xiao, S. Liang, and X. Zhang, 2016: Consistent estimation of multiple parameters from MODIS top of atmosphere reflectance data using a coupled soil-canopy-atmosphere radiative transfer model. *Remote Sens. Environ.*, **184**, 40–57, <https://doi.org/10.1016/j.rse.2016.06.008>.
- , ——, ——, and H. Ma, 2017: A method for consistent estimation of multiple land surface parameters from MODIS top-of-atmosphere time series data. *IEEE Trans. Geosci. Remote Sens.*, **55**, 5158–5173, <https://doi.org/10.1109/TGRS.2017.2702609>.
- Song, L., and Coauthors, 2018: Monitoring and validating spatially and temporally continuous daily evaporation and transpiration at river basin scale. *Remote Sens. Environ.*, **219**, 72–88, <https://doi.org/10.1016/j.rse.2018.10.002>.
- Song, Z., S. Liang, D. Wang, Y. Zhou, and Y. Yu, 2018: Long-term record of top-of-atmosphere albedo over land generated from AVHRR data. *Remote Sens. Environ.*, **211**, 71–88, <https://doi.org/10.1016/j.rse.2018.03.044>.
- Sun, Y., D. Wendi, D. E. Kim, and S.-Y. Liong, 2016: Development and application of an integrated hydrological model for Singapore freshwater swamp forest. *Procedia Eng.*, **154**, 1002–1009, <https://doi.org/10.1016/j.proeng.2016.07.589>.
- Tang, H., K. Yu, O. Hagolle, K. Jiang, X. Geng, and Y. Zhao, 2013: A cloud detection method based on a time series of MODIS surface reflectance images. *Int. J. Digital Earth*, **6**, 157–171, <https://doi.org/10.1080/17538947.2013.833313>.
- Tesemma, Z. K., Y. Wei, M. C. Peel, and A. W. Western, 2015: The effect of year-to-year variability of leaf area index on variable infiltration capacity model performance and simulation of runoff. *Adv. Water Resour.*, **83**, 310–322, <https://doi.org/10.1016/j.advwatres.2015.07.002>.
- Tian, X., and Coauthors, 2015: Simulation of forest evapotranspiration using time-series parameterization of the Surface Energy Balance System (SEBS) over the Qilian Mountains. *Remote Sens.*, **7**, 15822–15843, <https://doi.org/10.3390/rs71215806>.
- , and Coauthors, 2017: Modeling forest above-ground biomass dynamics using multi-source data and incorporated models: A case study over the Qilian Mountains. *Agric. For. Meteorol.*, **246**, 1–14, <https://doi.org/10.1016/j.agrformet.2017.05.026>.
- Verma, M., and Coauthors, 2015: Improving the performance of remote sensing models for capturing intra- and inter-annual variations in daily GPP: An analysis using global FLUXNET tower data. *Agric. For. Meteorol.*, **214–215**, 416–429, <https://doi.org/10.1016/j.agrformet.2015.09.005>.
- Wang, D., and S. Liang, 2016: Estimating high-resolution top of atmosphere albedo from Moderate Resolution Imaging Spectroradiometer data. *Remote Sens. Environ.*, **178**, 93–103, <https://doi.org/10.1016/j.rse.2016.03.008>.
- , and ——, 2017: Estimating top-of-atmosphere daily reflected shortwave radiation flux over land from MODIS data. *IEEE Trans. Geosci. Remote Sens.*, **55**, 4022–4031, <https://doi.org/10.1109/TGRS.2017.2686599>.
- Wang, H., and Coauthors, 2018: Sensitivity of biogenic volatile organic compound emissions to leaf area index and land cover in Beijing. *Atmos. Chem. Phys.*, **18**, 9583–9596, <https://doi.org/10.5194/acp-18-9583-2018>.
- Wang, J., J. Wang, H. Zhou, and Z. Xiao, 2017: Detecting forest disturbance in northeast China from GLASS LAI time series data using a dynamic model. *Remote Sens.*, **9**, 1293, <https://doi.org/10.3390/rs9121293>.
- Wang, K. C., R. E. Dickinson, M. Wild, and S. Liang, 2010: Evidence for decadal variation in global terrestrial evapotranspiration between 1982 and 2002: 1. Model development. *J. Geophys. Res. Atmos.*, **115**, D20112, <https://doi.org/10.1029/2009JD013671>.
- Wang, L., H. Zhu, A. Lin, L. Zou, W. Qin, and Q. Du, 2017: Evaluation of the latest MODIS GPP products across multiple biomes using global eddy covariance flux data. *Remote Sens.*, **9**, 418, <https://doi.org/10.3390/rs9050418>.
- Wang, Q., H. Zheng, X. Zhu, and G. Yu, 2015: Primary estimation of Chinese terrestrial carbon sequestration during 2001–2010. *Sci. Bull.*, **60**, 577–590, <https://doi.org/10.1007/s11434-015-0736-9>.
- Wang, R., J. M. Chen, Z. Liu, and A. Arain, 2017: Evaluation of seasonal variations of remotely sensed leaf area index over five evergreen coniferous forests. *ISPRS J. Photogramm. Remote Sens.*, **130**, 187–201, <https://doi.org/10.1016/j.isprsjprs.2017.05.017>.
- Wild, M., and Coauthors, 2014: The energy balance over land and oceans: An assessment based on direct observations and CMIP5 climate models. *Climate Dyn.*, **44**, 3393–3429, <https://doi.org/10.1007/s00382-014-2430-Z>.

- Xiao, Z., S. Liang, J. D. Wang, P. Chen, X. J. Yin, L. Q. Zhang, and J. L. Song, 2014: Use of general regression neural networks for generating the GLASS leaf area index product from time-series MODIS surface reflectance. *IEEE Trans. Geosci. Remote Sens.*, **52**, 209–223, <https://doi.org/10.1109/TGRS.2013.2237780>.
- , ——, T. Wang, and Q. Liu, 2015a: Reconstruction of satellite-retrieved land-surface reflectance based on temporally-continuous vegetation Indices. *Remote Sens.*, **7**, 9844–9864, <https://doi.org/10.3390/rs70809844>.
- , ——, R. Sun, J. Wang, and B. Jiang, 2015b: Estimating the fraction of absorbed photosynthetically active radiation from the MODIS data based GLASS leaf area index product. *Remote Sens. Environ.*, **171**, 105–117, <https://doi.org/10.1016/j.rse.2015.10.016>.
- , ——, J. Wang, D. Xie, J. Song, and R. Fensholt, 2015c: A framework for the consistent estimation of leaf area index, fraction of absorbed photosynthetically active radiation and surface albedo from MODIS time series data. *IEEE Trans. Geosci. Remote Sens.*, **53**, 3178–3197, <https://doi.org/10.1109/TGRS.2014.2370071>.
- , T. Wang, S. Liang, and R. Sun, 2016a: Estimating the fractional vegetation cover from GLASS leaf area index product. *Remote Sens.*, **8**, 337, <https://doi.org/10.3390/rs8040337>.
- , S. Liang, T. Wang, and B. Jiang, 2016b: Retrieval of leaf area index (LAI) and fraction of absorbed photosynthetically active radiation (FAPAR) from VIIRS time-series data. *Remote Sens.*, **8**, 351, <https://doi.org/10.3390/rs8040351>.
- , ——, J. Wang, Y. Xiang, X. Zhao, and J. Song, 2016c: Long-time-series Global Land Surface Satellite leaf area index product derived from MODIS and AVHRR surface reflectance. *IEEE Trans. Geosci. Remote Sens.*, **54**, 5301–5318, <https://doi.org/10.1109/TGRS.2016.2560522>.
- , ——, and B. Jiang, 2017a: Evaluation of four long time-series global leaf area index products. *Agric. For. Meteorol.*, **246**, 218–230, <https://doi.org/10.1016/j.agrformet.2017.06.016>.
- , ——, X. Tian, K. Jia, Y. Yao, and B. Jiang, 2017b: Reconstruction of long-term temporally continuous NDVI and surface reflectance from AVHRR data. *IEEE J. Sel. Top. Appl. Earth Obs. Remote Sens.*, **10**, 5551–5568, <https://doi.org/10.1109/JSTARS.2017.2744979>.
- , ——, and R. Sun, 2018: Evaluation of three long time series for global fraction of absorbed photosynthetically active radiation (FAPAR) products. *IEEE Trans. Geosci. Remote Sens.*, **56**, 5509–5524, <https://doi.org/10.1109/TGRS.2018.2818929>.
- Xu, B., and Coauthors, 2018: An integrated method for validating long-term leaf area index products using global networks of site-based measurements. *Remote Sens. Environ.*, **209**, 134–151, <https://doi.org/10.1016/j.rse.2018.02.049>.
- Xu, X., and Coauthors, 2013: Implications of ice storm damages on the water and carbon cycle of bamboo forests in southeastern China. *Agric. For. Meteorol.*, **177**, 35–45, <https://doi.org/10.1016/j.agrformet.2013.04.005>.
- Yang, L., K. Jia, S. Liang, J. Liu, and X. Wang, 2016: Comparison of four machine learning methods for generating the GLASS fractional vegetation cover product from MODIS data. *Remote Sens.*, **8**, 682, <https://doi.org/10.3390/rs8080682>.
- , S. Liang, and Y. Zhang, 2020: A new method for generating a global forest aboveground biomass map from multiple high-level satellite products and ancillary information. *IEEE J. Sel. Top. Appl. Earth Obs. Remote Sens.*, **13**, 2587–2597, <https://doi.org/10.1109/JSTARS.2020.2987951>.
- Yang, W., Y. Wang, X. Liu, H. Zhao, R. Shao, and G. Wang, 2020: Evaluation of the rescaled complementary principle in the estimation of evaporation on the Tibetan Plateau. *Sci. Total Environ.*, **699**, 134367, <https://doi.org/10.1016/j.scitotenv.2019.134367>.
- Yao, Y., and Coauthors, 2013: MODIS-driven estimation of terrestrial latent heat flux in China based on a modified Priestley-Taylor algorithm. *Agric. For. Meteorol.*, **171**, 187–202, <https://doi.org/10.1016/j.agrformet.2012.11.016>.
- , and Coauthors, 2014: Bayesian multimodel estimation of global terrestrial latent heat flux from eddy covariance, meteorological, and satellite observations. *J. Geophys. Res. Atmos.*, **119**, 4521–4545, <https://doi.org/10.1002/2013JD020864>.
- Yu, T., R. Sun, Z. Q. Xiao, Q. Zhang, J. M. Wang, and G. Liu, 2018: Generation of high resolution vegetation productivity from a downscaling method. *Remote Sens.*, **10**, 1748, <https://doi.org/10.3390/rs10111748>.
- Yuan, W., and Coauthors, 2007: Deriving a light use efficiency model from eddy covariance flux data for predicting daily gross primary production across biomes. *Agric. For. Meteorol.*, **143**, 189–207, <https://doi.org/10.1016/j.agrformet.2006.12.001>.
- , and Coauthors, 2010: Global estimates of evapotranspiration and gross primary production based on MODIS and global meteorology data. *Remote Sens. Environ.*, **114**, 1416–1431, <https://doi.org/10.1016/j.rse.2010.01.022>.
- , and Coauthors, 2014: Global comparison of light use efficiency models for simulating terrestrial vegetation gross primary production based on the LaThuile database. *Agric. For. Meteorol.*, **192–193**, 108–120, <https://doi.org/10.1016/j.agrformet.2014.03.007>.
- , and Coauthors, 2019: Increased atmospheric vapor pressure deficit reduces global vegetation growth. *Sci. Adv.*, **5**, eaax1396, <https://doi.org/10.1126/SCIADV.AAX1396>.
- Zeng, Q., J. Cheng, and L. Dong, 2020: Assessment of the long-term high-spatial resolution Global Land Surface Satellite (GLASS) surface longwave radiation product using ground measurements. *IEEE J. Sel. Top. Appl. Earth Obs. Remote Sens.*, **13**, 2032–2055, <https://doi.org/10.1109/JSTARS.2020.2992472>.
- Zhang, X., S. Liang, G. Zhou, H. Wu, and X. Zhao, 2014: Generating Global Land Surface Satellite incident shortwave radiation and photosynthetically active radiation products from multiple satellite data. *Remote Sens. Environ.*, **152**, 318–332, <https://doi.org/10.1016/j.rse.2014.07.003>.
- , and Coauthors, 2019: An operational approach for generating the global land surface downward shortwave radiation product from MODIS data. *IEEE Trans. Geosci. Remote Sens.*, **57**, 4636–4650, <https://doi.org/10.1109/TGRS.2019.2891945>.
- Zhang, Y., and S. Liang, 2014: Surface radiative forcing of forest disturbances over northeastern China. *Environ. Res. Lett.*, **9**, 024002, <https://doi.org/10.1088/1748-9326/9/2/024002>.
- , and ——, 2018: Impacts of land cover transitions on surface temperature in China based on satellite observations. *Environ. Res. Lett.*, **13**, 024010, <https://doi.org/10.1088/1748-9326/aa9e93>.
- Zhao, L., Z.-L. Yang, and T. J. Hoar, 2016: Global soil moisture estimation by assimilating AMSR-E brightness temperatures in a coupled CLM4–RTM–DART system. *J. Hydrometeorol.*, **17**, 2431–2454, <https://doi.org/10.1175/JHM-D-15-0218.1>.
- Zhao, X., and Coauthors, 2013: The Global Land Surface Satellite (GLASS) remote sensing data processing system and products. *Remote Sens.*, **5**, 2436–2450, <https://doi.org/10.3390/rs5052436>.
- Zheng, Y., and Coauthors, 2020: Improved estimate of global gross primary production for reproducing its long-term variation, 1982–2017. *Earth Syst. Sci. Data*, **12**, 2725–2746, <https://doi.org/10.5194/essd-12-2725-2020>.
- Zhou, J., S. Liang, J. Cheng, Y. Wang, and J. Ma, 2019: The GLASS land surface temperature product. *IEEE J. Sel. Top. Appl. Earth Obs. Remote Sens.*, **12**, 493–507, <https://doi.org/10.1109/JSTARS.2018.2870130>.
- Zhu, H., A. Lin, L. Wang, Y. Xia, and L. Zou, 2016: Evaluation of MODIS gross primary production across multiple biomes in China using eddy covariance flux data. *Remote Sens.*, **8**, 395, <https://doi.org/10.3390/rs8050395>.
- Zhu, Z., and Coauthors, 2016: Greening of the Earth and its drivers. *Nat. Climate Change*, **6**, 791–795, <https://doi.org/10.1038/nclimate3004>.